A computational fluid dynamics study of mass transfer in a large-scale aerated stirred bioreactor

Jamshidian, Roya; Scully, James; Van den Akker, Harry E.A.

DOI
10.1016/j.cej.2025.160723

Publication date
2025

Document Version
Final published version

Published in
Chemical Engineering Journal

Citation (APA)
Jamshidian, R., Scully, J., & Van den Akker, H. E. A. (2025). A computational fluid dynamics study of mass transfer in a large-scale aerated stirred bioreactor. *Chemical Engineering Journal*, *509*, Article 160723. https://doi.org/10.1016/j.cej.2025.160723

Chemical Engineering Journal 509 (2025) 160723

Contents lists available at ScienceDirect

Chemical Engineering Journal

journal homepage: www.elsevier.com/locate/cej

A computational fluid dynamics study of mass transfer in a large-scale aerated stirred bioreactor☆

Roya Jamshidian [a], James Scully [d], Harry E.A. Van den Akker [a,b,c,*]

[a] SFI Research Institute for Pharmaceutical Research (SSPC), University of Limerick, Limerick V94T9PX, Ireland
[b] Bernal Institute, School of Engineering, University of Limerick, Limerick V94T9PX, Ireland
[c] Department of Chemical Engineering, Delft University of Technology, Delft, Netherlands
[d] Regeneron Ireland DAC, Raheen Business Park, Limerick, Ireland

ARTICLE INFO

Keywords:
Finite Volume
Lattice Boltzmann
Energy dissipation rate
Bubble diameter
Volumetric mass transfer coefficient
Breakup and coalescence

ABSTRACT

Computational Fluid Dynamics (CFD) is exploited to study mass transfer in a specific stirred aerated bioreactor used in a cell culture process. The focus is on which empirical correlations from the literature can best be used for calculating the volumetric mass transfer coefficient k_La on the basis of the spatially distributed and/or average energy dissipation rate obtained in CFD simulations. This energy dissipation rate plays a key role in many of the empirical correlations which are reviewed in detail. CFD simulations are carried out using the finite volume (FV) ANSYS Fluent software as well as the Lattice Boltzmann (LB)-based code marketed by M−Star. In Fluent, we opted for a two-fluid approach and the realizable $k-\varepsilon$ turbulence model, while M−Star models the turbulence by a Large Eddy Simulation and tracks individual bubbles in a Lagrangian way. Gassed power draw, air volume fraction, energy dissipation rate, and (k_La) are calculated in both codes and compared mutually as well as to experimentally measured data and analytical correlations available in the literature. The energy dissipation rate was underpredicted by Fluent, leading to lower breakup rates and an underprediction of k_La. The M−Star simulations also underpredict k_La although predicting much higher levels of energy dissipation. However, using a constant value for k_L and just the volume-averaged a from Fluent or M−Star improved the results significantly, which then are in good agreement with the experimental k_La value.

1. Introduction

1.1. Rationale of the reported research

Mammalian cell culture processes are used in many pharmaceutical companies to produce monoclonal antibodies (*mAb*) by Chinese Hamster Ovary (CHO) cells. The cell culture process for manufacturing these *mAb* usually takes place in aerated stirred vessels of varying types and sizes. There is a wealth of research papers, both experimental and computational, on aerated stirred vessels, but mostly for vessels of limited size, restricted to (turbulent) flow fields only, and driven by a Rushton turbine or a Pitched Blade Impeller. In spite of this rich source of data, there is sufficient reason to further explore how to simulate the flow fields in bioreactors, usually provided with multiple profiled impellers, in our case dual elephant-ear impellers – also given the ever-increasing computational power, among which the use of GPUs.

One of the challenges of investigating particularly a *large-scale* bioreactor is in assessing and controlling important parameters such as mass transfer, dissolved oxygen concentrations, and strain rates, which are highly relevant for the intended growth of the CHO cells. During the operation of a commercial large-scale bioreactor, it is virtually impossible to extract reliable local and volume-averaged data about these parameters by using probes. Even the size of the bubbles in bioreactors is usually unknown. A common approach is to use empirical correlations, particularly for the volumetric mass transfer coefficient, k_La, found in the literature. Although usually such correlations have been obtained for different types of impellers, at smaller scales, and under different operating conditions, they are often used, also in computational studies, for want of something better.

Given the challenges involved in measuring the (overall) k_La value in bioreactors under live operating conditions, Computational Fluid Dynamics (CFD) techniques may provide an alternative [1], as CFD claims to resolve the flow field in quite some detail. CFD has been around for a

☆ This article is part of a special issue entitled: 'Guy Marin SI' published in Chemical Engineering Journal.

* Corresponding author.
E-mail address: harry.vandenakker@ul.ie (H.E.A. Van den Akker).

https://doi.org/10.1016/j.cej.2025.160723

Available online 17 February 2025

Nomenclature

a	Interfacial area ($m^{-1)}$
C_{exp}	Volume fraction correction coefficient (−)
C_D	Drag coefficient (−)
D	Impeller diameter (m)
D_L	Gas-liquid diffusion coefficient ($m^2.s^{-1)}$
d_0	Orifice diameter (m)
d_B	Bubble diameter (m)
d_{32}	Sauter mean diameter (m)
$d_{B,i}$	Initial bubble diameter (m)
f	Impeller frequency (Hz)
g	Gravitational acceleration ($m.s^{-2)}$
H_l	Liquid height (m)
k	Turbulent kinetic energy ($m^2.s^{-2)}$
k_L	Liquid side mass transfer coefficient ($m.s^{-1)}$
k_La	Volumetric mass transfer coefficient ($s^{-1)}$
N	Impeller rotational velocity (RPM)
$N_{P,\varepsilon}$	Power number based on energy dissipation rate (−)
$N_{P,t}$	Power number based on torque (−)
$N_{P,u}$	Ungassed power number (−)
P_ε	Power dissipated inside the tank (W)
P_g	Gassed power draw (W)
P_t	Gassed power draw based on torque (W)
P_u	Ungassed power draw (W)
Q	Volumetric gas flow rate ($m^3.s^{-1)}$
Re_B	Bubble Reynolds number (−)
s	Surface renewal rate (s^{-1})
T	Tank diameter (m)
t_e	Exposure (contact) time (s)
U_t	Terminal Velocity ($m.s^{-1)}$
U_{tip}	Impeller tip velocity ($m.s^{-1}$)
u	Velocity ($m.s^{-1}$)
u_s	Slip velocity ($m.s^{-1}$)
V	Working volume of liquid in the tank ($m^{3)}$
V_{cell}	Computational cell volume (m^3)
V_I	Volume swept by the impeller (m^3)
v_s	Superficial velocity ($m.s^{-1}$)
w	Impeller blade width (m)

Greek symbols

α_m	The volume fraction of phase m (−)
Δx	Computational cell/lattice size (m)
μ	Dynamic viscosity ($Ns.m^{-2)}$
ν	Kinematic viscosity ($m^2.s^{-1)}$
ω	Specific turbulent dissipation rate (s^{-1})
ρ_m	The density of phase m ($kg.m^{-3}$)
σ	Surface tension ($N.m^{-1)}$
τ	Torque (N.m)
ε	Turbulent energy dissipation rate ($m^2.s^{-3}$)

Subscripts

g	gas
l	liquid

few decades now and is a vastly explored technique for studying spatially resolved flow dynamics and associated operating parameters also in aerated stirred (bio)reactors. As a result, CFD could be used to learn about mass transfer and spatial distributions of k_L, a, and k_La, in cases for which no experimental data are available [1]. One of the goals of the research reported in this paper was to assess whether the current status of CFD for two-phase flows allows for a reliable prediction of k_L, a, and k_La and their spatial distributions, with the eventual goal of determining *in silico* the effect of optimising and/or dynamically varying operating conditions such as impeller speed and aeration rate.

Traditionally, various methods have been developed to measure this k_La, such as chemical methods, dynamic methods, etc. (see *e.g.*, Garcia Ochoa and Gomez [2]), each with its own benefits and drawbacks. A popular method exploits a single probe that interferes with the flow and yields only a single k_La value, often interpreted as a representative volume-averaged parameter. CFD techniques may then be used to substitute for measurements – with the drawback that validation of the computational values is not possible just due to the lack of measured data. Moreover, most experimental methods as used in stirred vessels, only provide the composite parameter, k_La, rather than separate values for the liquid-side mass transfer coefficient, k_L, and the specific interfacial area, a.

This paper focuses on how to arrive at confident estimates of mass transfer rates while presuming we can obtain optimum CFD representations of the turbulent flow field in a *large-scale* aerated bioreactor. To this purpose, the current study compares a Finite Volume (FV) method and a Lattice Boltzmann (LB) approach to simulate the two-phase flow field in an aerated stirred *large-scale* bioreactor with the view of finding values for the spatially distributed and overall mass transfer parameters. Results found through two-fluid RANS-based FV simulations with ANSYS/Fluent are compared with findings obtained from LESs with M−Star's LB software as well as with empirical correlations and own data for power draw and k_La.

1.2. CFD as a workhorse

The topic of CFD in general, and of two-phase CFD in particular, has fascinated many researchers for decades and CFD is applied within the industry for a wide variety of processes (among which aerated bioreactors). One of the first CFD papers on aerated stirred vessels was due to Bakker and Van den Akker [3] who used a heuristic model for the motion of the bubbles superimposed on a liquid flow field calculated with Fluent. Later on, two-fluid models were explored by *e.g.*, Lane et al. [4] and Khopkar et al. [5,6]. Some ten years ago, M−Star's software for Large Eddy Simulations (LESs) came onto the market. It builds on the 1999 paper by Derksen and Van den Akker [7] by exploiting the lattice Boltzmann (LB) technique. Generally, LESs which are inherently transient, provide a much more accurate description of the dynamics of turbulent flows [8]. For simulating two-phase flows, M−Star takes refuge in a Lagrangian approach that tracks the paths of individual bubbles by treating them as point particles subject to fluid-particle forces.

Given the extensive CFD database on stirred vessels (including earlier work from the Van den Akker group in Delft) and our recent paper [9] on lab-scale bioreactors, we are confident that our CFD two-phase flow fields allow for a detailed assessment of mass transfer models and correlations. Therefore, we will not validate the simulated turbulent flow fields here. This paper focuses on mass transfer and explores which correlations from the literature can reliably be used in CFD simulations to determine k_La. In Section 2.2, we briefly review the CFD literature on stirred vessels to explain our choices in turbulent flow field simulations.

More specific aspects, such as the correct bubble size (distribution) and the choice of the correlations for k_L and/or k_La, do deserve a thorough evaluation before their computational results can be trusted by *e.g.*, the pharmaceutical industry for application in simulating aerated and agitated bioreactors. To this end, we explored the use of population balances in Fluent by testing two different sets of models (*i.e.*, Luo for breakup and coalescence *vs.* Laakkonen for breakup combined with

Prince & Blanch for coalescence) with respect to their effects on power draw under gassed conditions, energy dissipation rate, bubble size, and k_La. In M−Star, the default unified model for the breakup and critical Reynolds model for coalescence was used with the initial bubble diameter being varied; *viz.* 1.8 mm, 3.54 mm, and 7.2 mm. The numerical results from the two codes were then compared to each other, to the available theoretical correlations and to our few experimental k_La value.

Such a thorough assessment is more relevant and even highly needed, as – also in the current study – very limited experimental data (only power draw and overall k_La) are available to validate the variables of interest including their spatial distributions. As a matter of fact, this scarcity of experimental data, certainly for large vessels provided with dual elephant-ear impellers, is exactly the reason for us in this paper as well as for the pharmaceutical industry, why refuge is taken to CFD techniques.

1.3. Structure of the paper

This paper is structured as follows: In Section 2, a literature review is presented which, in line with our focus on mass transfer, first addresses the topic of mass transfer in aerated stirred vessels in Section 2.1, and then concisely reviews the CFD of stirred vessels. Similarly, Section 3 on the modelling approach does not reproduce all equations typical of two-fluid CFD; it only reports some specific aspects of Fluent (in Section 3.1), of M−Star (in Section 3.2) and of power draw and dissipation (in Section 3.3). Then, Section 4 presents the input data and all technical details of the CFD simulations with both Fluent and M−Star. In Section 5, we present computational results for power draw, energy dissipation rates, air volume fractions and, eventually, volumetric mass transfer coefficient k_La. Finally, the conclusions follow in Section 5.

2. Literature review

2.1. Mass transfer

2.1.1. General remarks

We distinguish between two possible routes (see Fig. 1) for arriving at (averaged) values for k_La : starting from any flow field obtained by CFD, we may pursue either an approach resulting in spatially varying information on energy dissipation rate ε, bubble size, k_L and eventually k_La, or a route via the overall (or average) power draw under gassed conditions towards volume averaged values for bubble size and/or k_La. In both routes, empirical correlations are exploited, which were derived from conceptual models (often based on penetration theory) along with experimental investigations. Although these empirical correlations were obtained for different impeller types and different vessel sizes, they are included here as a type of yardstick for our computational results and to show their inadequacy outside the range of the experimental conditions for which were determined. Below, we present a detailed review of the various models for k_L, interfacial area a, and k_La.

While most of these correlations are in terms of power draw (under gassed conditions) or the dissipation rate ε of turbulent kinetic energy, they stem from the pre-CFD era and were never designed or intended (by *e.g.*, Hinze, or Higbie) to be used in a CFD code for calculating local values of bubble size, k_L, and k_La on the basis of local values of ε. In the period these models and correlations were derived, they generally were invoked to calculate vessel volume averaged parameter values. Now, CFD codes apply these models and correlations locally, assuming that bubble size responds to spatial ε-variations instantaneously, *i.e.* with a response time equal to zero. However, Mukherjee et al. [10] found that (local) drop size in agitated emulsions lags behind spatial variations in ε.

2.1.2. Liquid-side mass transfer coefficient

All models for the liquid-side mass transfer coefficient, k_L, in any dispersed gas–liquid flow are based on the classical concept of pene-

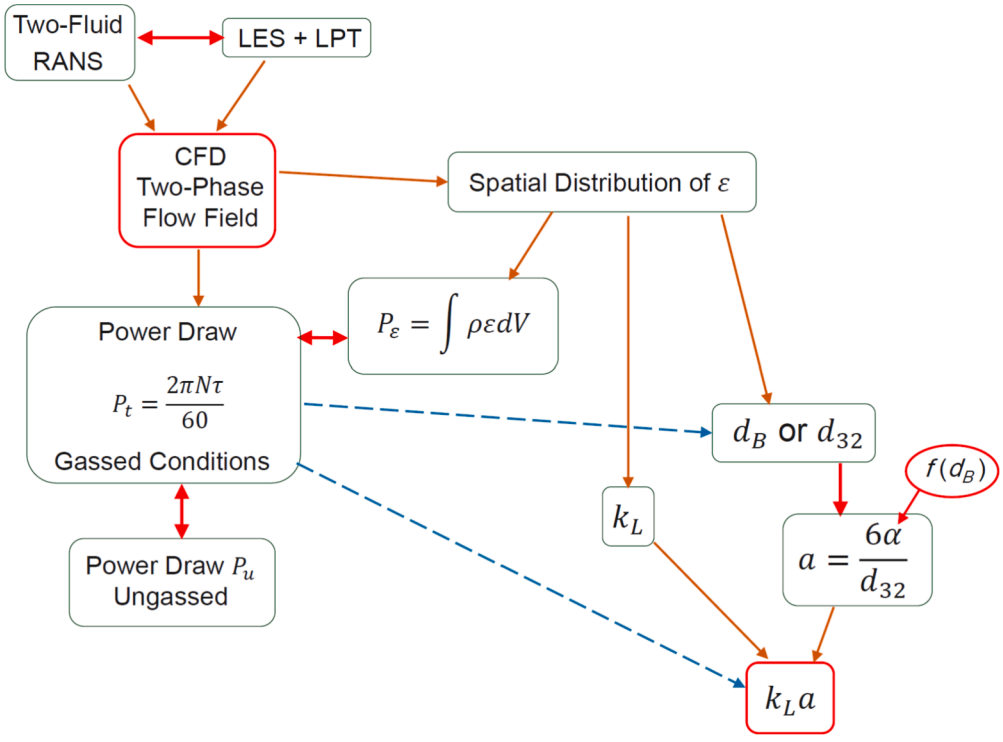

Fig. 1. Illustrating the two possible routes starting from any CFD obtained flow field ((upper left corner): **(a)** the (red) route (at the right-hand side) resulting in spatially varying information on ε, bubble size and eventually k_La; **(b)** the route with the (blue) broken lines, starting from the power draw under gassed conditions and resulting in volume averaged values for bubble size and/or k_La. The double-headed arrows are indicative of comparisons and assessments of the boxed parameters. (For interpretation of the references to colour in this figure legend, the reader is referred to the web version of this article.)

Table 1
Correlations defined in the literature for calculating the liquid-side mass transfer coefficient (k_L).

Author	Model	Correlation
Higbie [11]	Penetration into a steady film flow	$k_L = 2\sqrt{\frac{D_L}{\pi t_e}}$
Danckwerts [15]	Surface renewal	$k_L = \sqrt{D_L s}$
Calderbank [16]	Slip velocity	$k_L = \frac{2}{\sqrt{\pi}}\sqrt{\frac{D_L u_s}{d_B}}$
Alves et al. [17]	Rigid model	$k_L = c\left(\frac{u_s}{d_B}\right)^{1/2} D_L^{2/3}\nu^{-1/6}$
Lamont and Scott [19]	Eddy cell	$k_L = 0.4\sqrt{D_L}\left(\frac{\varepsilon}{\nu}\right)^{0.25}$
Kawase and Moo-Young [21]	Using Kolmogorov time scale	$k_L = 0.301\sqrt{D_L}\left(\frac{\varepsilon}{\nu}\right)^{0.25}$

tration theory. The essential question then is to find an appropriate value for the exposure time and how it may depend on the local fluid dynamics at the point of contact. Many papers refer to Higbie [11] who used penetration theory to model mass transfer between a gas and a film flow over a distinct distance of contact, see *e.g.*, Bird et al. [12], Cussler [13], and Welty et al. [14].

Under turbulent flow conditions around a gas bubble, the exposure or contact time is less well-defined. Danckwerts [15] developed a model for k_L based on the concept of a surface renewal rate, s, expressing that the bubble interface is exposed to turbulent eddies. Calderbank [16] assumed the bubble to have a mobile surface and the mean relative liquid flow (slip velocity) to control the surface renewal. He expressed the exposure time in terms of an average bubble size and an average slip velocity. Alves et al. [17] further modified the Calderbank equation based on the bubble rigidity and used the equation proposed by Frössling [18] to obtain the rigid model for calculating k_L.

Lamont and Scott [19] introduced the so-called eddy cell model that postulates surface renewal by turbulent eddies is the controlling mechanism of mass transfer from bubbles travelling co-currently with liquid in a horizontal pipe. Kawase et al. [20] used the Kolmogorov time scale of isotropic turbulence to define the exposure time of classical penetration theory, giving the correlation for k_L, the shape commonly used: with the (local or volume-averaged) energy dissipation rate, ε. Kawase and Moo-Young [21] estimated the exposure time based on a periodic translational sublayer model (Pinczewski and Sideman, [22]) and adopted their model. All these correlations are summarised in Table 1. A more detailed evaluation of these analytical models using CFD can be found elsewhere [23,24].

In another study, Calderbank and Moo-Young [25] claimed that k_L at a certain bubble size, only depends on the physical properties of the phases. They also concluded that in an aerated stirred vessel, k_L is independent of the bubble size, except in an intermediate range of bubble sizes, where the value of k_L depends on the bubble size and increases with it.

2.1.3. Specific interfacial area

In a similar way for k_L, correlations were developed to calculate the specific interfacial area. The most widely used correlation is based on the assumption that bubbles are spherical such that the interfacial area (a) is a simple function of gas holdup (α_g) and bubble diameter (d_B) (or Sauter mean diameter, d_{32}, in case of a bubble size distribution). Hänsch et al. [26] reported that the rate of coalescence increases sharply up to a critical gas holdup of $\alpha_g = 0.3$ beyond which the bubbly flow transitions to a resolved-structure flow. Based on this, they developed three different correlations for interfacial area depending on the local air volume fraction. Maluta et al. [27,28] used this approach in a number of their studies and found a great agreement between their experimental and their CFD $k_L a$.

All these correlations are shown in Table 2.

2.1.4. Volumetric mass transfer coefficient $k_L a$

The *volume-averaged* empirical correlations obtained in studies of Lamont and Scott [19], Kawase and Moo-Young [21], and Alves et al. [17], are widely employed in CFD simulations to compute *local* k_L and *local* $k_L a$ values using *spatially distributed local* ε values. We opted for Kawase and Moo-Young, as its derivation is more general, it is recommended by M−Star in their tutorial, and it can easily be applied in Fluent. Note, however, that using these correlations in a CFD context was already questioned at the start of this Section 2.1. Subsequently, the volume-averaged $k_L a$ is determined by averaging these local $k_L a$ values across the entire tank volume. Given the non-linear character of the correlations, this approach may be considered dubious as well.

Other attempts were made to develop an analytical engineering correlation that can be used for the calculation of the volumetric mass transfer coefficient. These correlations are usually in one of two categories using either dimensionless groups (*i.e.* Froude number, gas flow number, dimensionless impeller diameter, etc.) or an energy input criterion based on Kolmogorov's theory [16,29,30]. Most correlations for such a volume-averaged $k_L a$ prediction depends on $\frac{P_g}{V}$, P_g denoting the power draw under gassed conditions, and on the slip velocity, v_s, and are based on the assumption of isotropic turbulence:

$$k_L a = K_1 \left(\frac{P_g}{V}\right)^{K_2} v_s^{K_3} \tag{1}$$

Varying power exponents have been reported in the literature for K_1, K_2, and K_3, depending on impeller diameter and type. Some authors used unsuitable physical models and techniques for evaluating the experimental data, leading to problems in proposing a correlation for the mass transfer coefficient [31]. Interested readers can refer to the works of Linek et al. [32], Halveka et al. [33], and Labík et al. [34]. In several studies across the literature – *e.g.* Devi and Kumar [23]– the correlation defined by Van't Riet et al. [30] (also mentioned earlier by Calderbank [35]) has been used:

$$k_L a = 0.026 \left(\frac{P_g}{V}\right)^{0.4} v_s^{0.5} \tag{2}$$

Table 2
Correlations defined in literature for calculating specific interfacial area (a).

Author	Correlation
General	$a = \frac{6\alpha_g}{d_B}$
Hänsch et al. [26]	$a = \begin{cases} \frac{6\alpha_g}{d_B} & \text{for} \quad \alpha_g \le 0.3 \\ 4\pi\left(\frac{3}{4\pi}\alpha_g\right)^{\frac{2}{3}} / V_{Cell}^{\frac{1}{3}} & \text{for} \quad 0.3 < \alpha_g \le 0.5 \\ 4\pi\left(\frac{3}{4\pi}\alpha_l\right)^{\frac{2}{3}} / V_{Cell}^{\frac{1}{3}} & \text{for} \quad \alpha_g > 0.5 \end{cases}$

Note the exponent of $\frac{P_g}{V}$ is different from the exponent 0.25 of ε in the expressions due to Lamont and Scott and due to Kawase and Moo-Young in Table 1, while $\varepsilon = \frac{P_g}{\rho V}$. Such empirical equations are usually developed for a system with a Rushton turbine and therefore might not produce accurate results for reactors with other types of impellers.

More recently, Yawalkar et al. [36] defined a new correlation based on some relative gas dispersion parameter and found good results for k_La. In another empirical study, Petříček et al. [31] estimated the values of K_1, K_2, and K_3 for systems of single, dual, and three impellers and found the equation to be accurate enough to predict their k_La data.

Several researchers, including Calderbank and Moo-Young [25] and Farsani et al. [37], recommend using a constant k_L value, typically $5 \cdot 10^{-4}$ m/s. These studies suggest that variations in the energy dissipation rate do not directly impact k_L; instead, they influence the volumetric mass transfer coefficient by affecting bubble size and, consequently, the interfacial area. This constant value for k_L may be useful under standard operating conditions.

2.2. Computational fluid dynamics (CFD)

First of all, we used ANSYS/Fluent to simulate our aerated stirred vessel with the help of a two-fluid model combined with a Reynold Averaged Navier Stokes (RANS) approach, while we used the MRF technique to deal with the revolving impeller. The equations and other details of the two-fluid model and the turbulence model used can be found in Jamshidian et al. [9]. We will now focus on more specific aspects of our CFD simulations.

While the underprediction of the turbulent parameters by RANS turbulence models, known for a long time [8], was generally considered to be a typical feature of RANS-based simulations, some research studies blamed this on the use of coarser meshes and lower-order discretization schemes [38–40], though strictly speaking these findings relate to *single-phase* unaerated stirred reactors.

As k_La is highly dependent on bubble size, so the correct prediction of the bubble size (distribution) is important. Some simulations found using a single bubble size to be sufficient [23,41]. The question is, however, whether the bubbles during their rise and stay in the stirred reactor keep the size they got at the air distributor, or whether they are subjected to bubble–bubble and impeller-driven bubble-turbulence interactions resulting in a bubble size distribution, not to talk about their expansion during their rise in production-scale reactors. Bubbles break up when the local energy dissipation rate of the liquid exceeds the bubble's surface energy. Several models (with several empirical coefficients) are available to describe bubble break-up and bubble coalescence.

Most numerical simulation studies in the field of mass transfer use population balance methods (PBMs) [42–47] to capture a bubble size distribution (BSD). One study showed that increasing the number of bubble-size classes increases the accuracy of the model at the cost of higher computational demand [42]. The addition of a PBM to CFD models, although helpful in predicting mean bubble size and the volumetric mass transfer coefficient, can be computationally excessive if combined with the chemical reactions of a cell culture process.

The majority of the common FV CFD solvers have limited compatibility with high-performance computing architectures such as Graphics Processing Units (GPUs) and therefore become restricting for transient simulations with prolonged run times [48,49]. Although GPUs were originally developed to accelerate graphics rendering and display, the localized nature of the Boltzmann transport equations is largely exploited in a GPU processing environment. This step change in computational speed in M−Star's CFD software is the reason for including in this paper the Large Eddy Simulation (LES) results obtained with this code.

M−Star−CFD is a recently introduced solver for performing LESs of a turbulent flow field. LESs resolve a large part of the turbulence spectrum while a Smagorinsky model captures the influence of the sub-grid scale (SGS) eddies with a length scale smaller than the lattice spacing. While in Fluent we used the Eulerian (or two-fluid) option for modelling the bubbles, M−Star uses a Lagrangian approach. In this method, the bubbles are tracked individually, and the mass and momentum conservation equations are solved for each bubble individually as well as for the liquid phase. Therefore, the Lagrangian approach is a computationally demanding method when a large number of bubbles are present. M−Star, however, has the advantage of using GPUs for the simulations, making it much faster than Fluent Lagrangian simulations.

The LB-based solver the flow field discretizes a Boltzmann transport equation onto a uniform lattice with regularly spaced nodes (or grid points). Then, fluid parcels are represented in terms of molecular probability density functions (PDFs) which experience a collision operation at the nodes before streaming toward neighbouring nodes. Together with the specified boundary conditions, these collision and streaming operations are governed by a discretized Boltzmann transport equation. From the spatial distributions of the PDFs, the density and velocity fields can be obtained. The concept of the transient LESs nicely combines with the dynamics of the LB technique. For more details, the reader is referred to *e.g.*, the early paper by Derksen and Van den Akker [7].

Additional reactor features such as species transport, mass transfer, and chemical reactions are resolved through a Lagrangian approach, just like for the bubbles. Thomas et al. [50,51] carried out several simulations exploring the ability of the software to predict the mass transfer coefficient and biological reactions happening in the cell culture process. Farsani et al. [37] pointed out that the mass transfer coefficient is invariant with the specific energy dissipation rate and found that assuming a constant mass transfer coefficient (same as Calderbank and Moo-Young, [25]) is the most conservative option from a robustness point of view. In general, M−Star seems to be very promising due to combining more realistic methods, *i.e.*, the Lagrangian method, rather than the two-fluid approach, to track bubbles in a turbulent flow regime using a high-accuracy dynamic large eddy turbulence model.

3. Modelling approach

3.1. Two-fluid simulation in Fluent

A two-fluid approach is employed for modelling the stirred aerated bioreactor in ANSYS/Fluent 2022R2. Based on this approach, the bubbles are not modelled individually but rather, they are conceived as a continuum phase interpenetrating the liquid phase. The mass and momentum conservation equations for this approach can be found in our previous paper [9]. The only interphase force taken into account is the drag force, where the drag coefficient is modelled using the Grace drag model [52]:

$$C_D = \alpha_g^{C_{exp}} \cdot \max\left[\min\left[C_{D_{ellipse}}, C_{D\,Cap}\right], C_{D_{sphere}}\right] \tag{3}$$

in which

$$C_{D_{ellipse}} = \begin{cases} 24/Re_B & \text{for} \quad Re_B < 0.01 \\ 24\left(1 + 0.15\,Re_B^{0.687}\right)/Re_B & \text{for} \quad Re_B \geq 0.01 \end{cases} \tag{4}$$

$$C_{DCap} = \frac{8}{3}$$

$$C_{D_{sphere}} = \frac{4}{3}\frac{gd_B}{U_t^2}\frac{\left(\rho_l - \rho_g\right)}{\rho_l}$$

In these equations, Re_B is the bubble Reynolds number:

$$Re_B = \frac{\rho_l \left|u_l - u_g\right| d_B}{\mu_l} \tag{5}$$

The reason for choosing this drag coefficient model is due to its sensitivity to the shape and size of the bubbles where the drag coefficient is calculated based on the shape regime (spherical, elliptical, cap-shaped). No turbulent drag modification model was used because our studies showed that the Brucato model overpredicts the gas holdup while the Lane model did not have a significant influence on the air volume fraction. Some studies such as Montante et al. [53], Maluta et al. [27,40,54,55], and Xing et al. [56] added a turbulent dispersion force to the simulations. Yet, an abundant number of studies are still carried out in Fluent with only drag being taken into account [57–62]. Therefore, this turbulent dispersion force was also not included in the current study.

The impeller rotation was modelled mainly by using the MRF method. As for the turbulence model, the realizable $k-\varepsilon$ model was used for modelling the turbulence flow. In general, the realizable $k-\varepsilon$ model performs better than the standard (or basic) $k-\varepsilon$ model that only can be used in combination with (simplified) wall functions. The realizable $k-\varepsilon$ turbulence model is also recommended for simulating stirred aerated bioreactors due to its improved predictions of the complex flow field and energy dissipation rates, and because of its compatibility with multi-phase flows, all while balancing accuracy and computational efficiency [63]. We also explored the SST $k-\omega$ model but this did not give better values for ε.

To model the bubble size distribution (BSD), the method of classes which is available in the PBM approach is used where 14 bubble classes are used and the initial bubble diameter is calculated using the equation obtained by Miller [64] on the basis of a simple force balance between buoyancy and surface tension:

$$d_B = \left(\frac{6\,\sigma\,d_0}{g(\rho_l-\rho_g)}\right)^{\frac{1}{3}} \tag{6}$$

Initially, the Luo model was used to model both breakup and coalescence [65,66], however, a second simulation was run using the Laakkonen model [42] for the breakup and the Prince and Blanch coalescence model [67].

The liquid-side mass transfer coefficient was calculated using the Kawase and Moo-Young correlation, previously mentioned in Table 1. The interfacial area is calculated with the help of the commonly used correlation for spherical bubbles (see Table 2).

3.2. Euler-Lagrange simulation in M-Star LESs

M−Star is an LB-based software in which the flow field is resolved on a lattice with regularly spaced grid points. The fluid is represented in terms of finite parcels carrying a molecular probability density function that undergoes a collision operation before streaming towards neighbouring points. The collision and streaming operations are governed by a discretized Boltzmann transport equation obeying appropriate boundary conditions. The interaction of the liquid with the rotating impeller is modelled by using an immersed boundary method (IBM). The turbulent flow is modelled with the help of the LES concept that exploits a filter the size of which is equal to the size of the computational cell (or the lattice spacing) such that all eddies larger than the filter size are resolved. The effect of the subgrid-scale (SGS) eddies (smaller than the filter size) on the larger scales of the turbulent flow field is modelled with the help of the Smagorinsky model, meaning that the SGS eddies remain unresolved. The Smagorinsky model introduces a subgrid viscosity related to the lattice spacing Δx according to

$$\nu_t = 2\,(C_S\Delta x)^2|\overline{S}| \tag{7}$$

where C_S is the Smagorinsky constant, equal to a default value of 0.1, $|\overline{S}|$ is the norm of the filtered strain rate tensor, and $\overline{S}_{ij}$ is the characteristic filtered strain rate obtained from the resolved velocity components. The effective fluid viscosity ν_e at each cell is the summation of the molecular viscosity (ν) and the subgrid Smagorinsky viscosity (ν_t):

$$\nu_e = \nu + \nu_t \tag{8}$$

Being a Lagrangian-based code, the bubbles are modelled as discrete point objects that can evolve according to Newton's second law. The interphase forces comprise a gravity/buoyancy force as well as drag and added mass forces. The position and velocity of each bubble are solved by integrating the acceleration vector over time using a Verlet algorithm with the same time-step defined for the description of the fluid flow. Therefore, for coupling the two phases, a local body force is applied to each fluid voxel per the local gas volume fraction. This method which is referred to as the density method is chosen due to its lower computational costs and being less complicated.

As a result of fluid shear force and the bubble–bubble collisions, the bubbles can undergo breakup and coalescence. Here, the bubble breakup is modelled using the unified model (interested readers can refer to Xing et al. [68]) where the breakup is assumed to only happen as a result of a collision with turbulent eddies. An essential element in the kernel used in M−Star is equation (9):

$$d_B = C\frac{\sigma^{3/5}}{\rho_l^{3/5}\varepsilon^{2/5}} \tag{9}$$

Where C is a constant that changes between 0.1–1.0, and σ denotes surface tension, equal to 0.072 Nm^{-1} for air bubbles in the water. Equation (9) stems from Hinze's critical Weber number correlation which, however, was in terms of a dynamic pressure rather than in terms of ε. This equation is obtained by exploiting Taylor's relation ($\varepsilon \sim u^3/\ell$) applied at the bubble scale (*i.e.*, $\ell \approx d$). It is very dubious, however, whether this approach is valid for bubbles in the mm range. Applying equation (9) locally requires a local value of the energy dissipation rate.

In this approach, only binary breakup is considered, since the probability of binary bubble breakup is typically larger than 95% [69,70]. To model the coalescence, a critical Reynolds method is used based on which the coalescence happens when the bubble Reynolds number exceeds the critical approach Reynolds number calculated from the approach velocity of two colliding bubbles.

Similar to Fluent, the mass transfer coefficient on the liquid side (k_L)

Table 3
Correlations used for calculating gassed power input from literature used in the current study as a reference.

Author	Correlation	Remarks
Michel and Miller [71]	$P_g = K_1\left(\frac{P_u^2 f D^3}{Q^{K_3}}\right)^{K_2}$	Abrardi et al. [72] for Rushton impellers: Single impeller: $K_1 = 0.783$, $K_2 = 0.459$, $K_3 = 0.56$ Dual impeller: $K_1 = 1.224$, $K_2 = 0.432$, $K_3 = 0.56$
Hughmark [73]	$P_g = K_1\left(\frac{N^2D^4}{g\,w\,V^{2/3}}\right)^{K_2}\left(\frac{Q}{NV}\right)^{K_3}$	Petříček et al. [31] for single, dual, and three impellers: $K_1 = 0.0012$, $K_2 = 0.71$, $K_3 = 0.9$ $K_1 = 0.1$, $K_2 = -0.2$, $K_3 = -0.25$
Petříček et al. [31]	$\frac{P_g}{V} = K_1\left(\frac{P_u}{V}\right)^{K_2} v_s^{K_3}$	$K_1 = 0.147$, $K_2 = 0.94$, $K_3 = -0.36$ from fitting experimental data

is calculated from the correlation defined by Kawase and Moo-Young. The interfacial area, however, is calculated as the local specific area of the bubbles and is reported automatically by the software. Then the multiplication of the interfacial area with the liquid side mass transfer coefficient provides the k_La which is reported locally and globally by the software.

3.3. Power draw and dissipation

As mentioned in Section 2.1, power input is a crucial characteristic of stirred aerated bioreactors as it affects bubble size, gas holdup, liquid-side mass transfer coefficient (k_L), and therefore, the volumetric mass transfer coefficient (k_La). As a result of this, many studies consider power input and/or define analytical correlations to calculate it. Given the low aeration rates, we will consider the power draw from the impeller as the only source of power input. Several correlations were developed to calculate the power draw (P_g) under gassed conditions which are shown in Table 3. These equations are used in the current study to compare with the gassed power input derived from the simulations. It is worth noting that the power exponents for this correlation are developed for a system with single, dual, and multiple combinations of RT, A315, and PBT impellers and discrepancies might be expected when compared to the results of the current CFD simulation for a system with dual elephant ear impellers.

To calculate the gassed power draw from CFD results, the correlation based on impeller torque (τ) and rotational speed (N, in RPM) is used. This correlation is defined as

$$P_t = \frac{2\pi N\tau}{60} \tag{10}$$

The usual practice is to compare the power draw (at the large scale) with the consumed and dissipated power ε. Energy dissipation takes place due to three main mechanisms, *viz.* in the turbulent motion, in the mean flow, and in the boundary layers at the vessel walls [74]. The total energy dissipation rate then follows from integrating the local values of ε over the flow domain:

$$P_\varepsilon = \int \rho\, \varepsilon\, dV \tag{11}$$

To calculate ε, M−Star requires a post-processing routine, because, differently from RANS models, ε is not a local variable needed for the flow simulation itself. The M−Star User manual reports that the resolved energy dissipation rate may be calculated by

$$\varepsilon_{res} = 2\nu \sum_{ij} \overline{S}_{ij}\overline{S}_{ij} \tag{12}$$

Which may be conceived as the rate of dissipation in the dynamic mean flow including that along the walls of the vessel. As for the energy dissipation rate associated with the unresolved SGS eddies, the M−Star User Manual specifies:

$$\varepsilon_{unres} = 2\nu_t \sum_{ij} \overline{S}_{ij}\overline{S}_{ij} = 2(C_S\Delta x)^2|\overline{S}|\sum_{ij} \overline{S}_{ij}\overline{S}_{ij} \tag{13}$$

M−Star does not report the separate (local or volume-averaged) values of the resolved and unresolved energy dissipation rates during or after a simulation. In general, $\nu_t \gg \nu$.

In line with the derivation presented by Gillissen and Van den Akker [75] with the view of their in-house LES code, Giacomelli and Van den Akker [76], who used M−Star, report an expression for the total (*i.e.*, resolved plus unresolved) energy dissipation rate:

$$\varepsilon = 2\nu_e \sum_{ij} \overline{S}_{ij}\overline{S}_{ij} \tag{14}$$

With ν_e given by equation (8). Equation (14) gives the same numerical value for the total energy dissipation rate as the sum of equations (12) and (13) but rather expresses that, due to the unresolved part of the turbulent flow field, an increased (or effective) viscosity should (or could) be used for calculating the total energy dissipation rate.

In the perception of the authors, equation (13) just represents the power *to be* dissipated at scales smaller than the filter size which in our simulations is of the order of a few cm. Classical turbulence theory, summarised in Richardson's rhyme about turbulent eddies feeding on each other and illustrated by the well-known turbulence spectrum, teaches that turbulent kinetic energy is dissipated in the Kolmogorov eddies (which in our cases are as small as 0.5 mm) because of the dominating role of viscosity. One may conceive equation (13) as expressing that the entire power drawn by the torque at the macro-scale is transported 'downwards' to the mesoscale of the filter size, the eventual destination being the Kolmogorov eddies where it will be dissipated into heat. Equation (13) relates to the domain of the resolved flow and does not say anything about the unresolved Kolmogorov time and length scales and the dissipation (rate) itself. The variable ε_{unres} is calculated in a post-processing routine and as such does not contribute to the simulation process.

This is quite different from RANS simulations in which ε is one of the flow variables to be calculated by the code itself given its relevance for the eddy viscosity and, hence, for the average flow field. In a RANS simulation, ε contributes to the solution of the turbulent flow field and can be truly conceived as representing the dissipation rate in the Kolmogorov eddies. It is noteworthy that this ε does not include the energy dissipation in the mean flow and along the vessel walls which are treated separately.

In a steady-state condition, the (gassed) power draw based on torque (P_t) is equal to the power consumption due to dissipation (P_ε). The value of the input power is usually reported using the power number. The power number based on the torque, $N_{P,t}$, experienced by the impeller (and shaft) was calculated for each case using the equation below.

$$N_{P,t} = \frac{P_t}{\rho\, N^3 D^5} \tag{15}$$

Similar to the power number based on the torque, the power number based on the energy dissipation rate can be calculated using:

$$N_{P,\varepsilon} = \frac{P_\varepsilon}{\rho\, N^3 D^5} \tag{16}$$

3.4. Sauter mean bubble

Bubble size has a significant effect on the accuracy of the volumetric mass transfer coefficients. The correlation defined by Miller, equation (6), predicts a bubble diameter based on the gas and liquid properties. It has been used in the current study to define the initial size of the bubbles for simulations with breakup and coalescence.

There are other correlations (Table 4), however, that are introduced for the calculation of the Sauter mean bubble size (d_{32}) inside a stirred aerated bioreactor. One of these correlations was defined by Calderbank [16] where the surface-based mean bubble diameter ($\overline{d}_{32}$) is a function of gassed input power (P_g). In another study, Alves et al. [77] defined

Table 4
Correlations defined in literature for calculating mean Sauter diameter in stirred aerated tank used in the current study.

Author	Correlation
Calderbank [16]	$\overline{d}_{32} = 4.15\, \frac{\sigma^{0.6}}{\left(\frac{P_g}{V}\right)^{0.4} \rho_L^{0.2}}\, \alpha_g^{0.5} + 0.0009$
Alves et al. [77]	$d_{32,ID} = 0.25 \left(\frac{P_g}{V_l}\right)^{-0.52}$ and $d_{32,B} = 0.0076 \left(\frac{P_g}{V}\right)^{-0.14}$

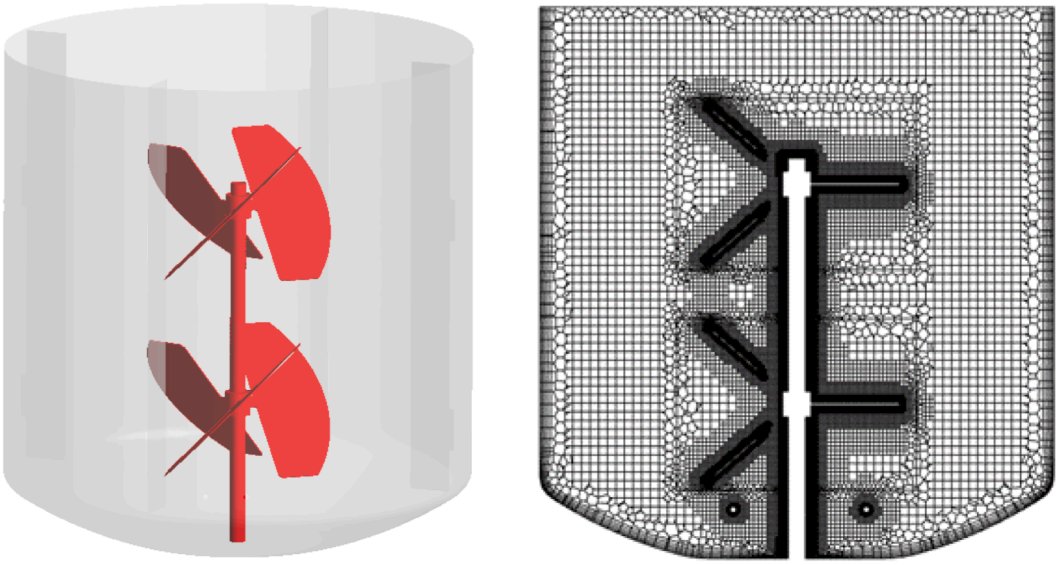

Fig. 2. **(a)** the schematic figure of the 10,000-litre tank (the sparger is not shown), **(b)** the mosaic mesh used for the current model.

two other correlations based on the gassed power number for calculating the mean Sauter diameter in the impeller discharge region ($d_{32,ID}$ in the impeller's swept volume V_I) and in the bulk of the liquid ($d_{32,B}$) in a coalescing system. Maluta et al. [27,28] used the correlation of Alves to model the bubble size in the impeller region and the bulk of their tank, separately.

In the current study, the Sauter mean diameter calculated from the simulation will be compared to the Sauter diameter calculated from these two analytical correlations.

4. Technical details of the simulations

4.1. Geometry and physical properties

This study is carried out on a 10,000-liter industrial baffled reactor with an internal diameter of $T = 2.286$ m filled with liquid up to $H_l = 2.59$ m. The four baffles are 0.203 m in width and are mounted onto the walls at a gap width of 25.4 mm. Two bottom-mounted 3-blade elephant-ear type impellers (Fig. 2-a) with a diameter of $D = 0.9144$ m agitate the liquid at a speed of 50 RPM. The lower impeller is at a distance of approximately 0.336 m above the vessel's bottom. The impeller power number has been measured to be 3 for a fully submerged state without aeration.

To supply gas as required, a hexagonal ring sparger is installed at a clearance of 0.217 m above the bottom of the reactor. The air is injected through a number of apertures in the left arm of this sparger at a rate of 250 SLPM (standard litre per minute) while the right-side arm does not participate in the aeration process. Further details of this sparger cannot be reported for proprietary reasons; given the very low aeration rate, resulting in maximum local air volume fractions of just 1%, these details do not really matter.

The liquid properties are $\rho_l = 990$ kg/m^3 and $\mu_l = 7.34 \cdot 10^{-4}$ Ns/m^2 and the air has properties of $\rho_g = 1.14$ kg/m^3 and $\mu_g = 1.891 \cdot 10^{-5}$ Ns/m^2. The diffusion coefficient of dissolved oxygen in the liquid is taken as $D_L = 2.01 \cdot 10^{-9}$ m^2/s.

For the majority of the cases investigated here in both Fluent and M−Star, a monodispersed model is considered, and the bubble size is calculated to be $d_B = 3.54$ mm using equation (6) [64]. Moreover, two other bubble sizes ($d_B = 1.8$ mm and $d_B = 7.2$ mm) are also used as a part of the sensitivity study.

4.2. Fluent simulation setup

In the current study, due to the large scale of the reactor being operated in an industrial setting, information about velocity field, gas holdup, bubble size distributions, *etc.* is not available. The only two parameters available are the ungassed power number of the impellers ($N_{P,u}$) obtained from the vendor as well as the volumetric mass transfer coefficient (k_La) which was measured experimentally.

4.2.1. Single-phase simulation

The parameter chosen for the grid independence study was the ungassed power number ($N_{P,u}$) of the impeller when the tank is running only with the liquid phase, *i.e.* without aeration. Overall, a mosaic grid was chosen for this study, and the domain around the impeller blades was refined by using a body of influence (BOI) with the view of the y^+ values. Acceptable y^+ values for the case of a RANS model simulations are generally suggested to be $30 < y^+ < 300$. In our study, the values of y^+ fall in the range of 150 - 280, depending on the settings. Four grid density numbers were checked: 2,066,767 cells (body of influence size: 0.008, 3 inflation layers), 3,889,328 cells (body of influence size: 0.004, 5 inflation layers), 17,794,318 cells (body of influence size: 0.002, 7 inflation layers), and 85,106,690 million cells (body of influence size: 0.001, 9 inflation layers) running for the single-phase case.

The discretization schemes used for the simulation of the single-phase bioreactor were 2nd-order for pressure and 2nd-order upwind for momentum and turbulent variables (k and ε). For the pressure–velocity coupling, a coupled method was used, and simulations were run as pseudo-transient using the default time-step of the code. The walls were modelled as no-slip except for the impeller which was rotating at 50 RPM, and the outlet was modelled using a symmetry boundary condition, with the impeller rotation modelled with the MRF method. The convergence for the three cases was obtained after around 20,000 iterations when the variations in energy dissipation rate and torque stayed within 1–2 %.

The power number based on the torque, $N_{P,t}$ - see equation (15) - is compared to the value of the power number for the unaerated fully submerged case ($N_{P,u}$) specified by the vendor. The values of the input power number were calculated to be 2.97, 3.02, 3.06, and 3.07 for the above-mentioned four grid densities, respectively.

The comparison of $N_{P,u}$ with the numerical value of $N_{P,t}$ and the numerical dissipated power from energy dissipation rate, $N_{P,\varepsilon}$ - see

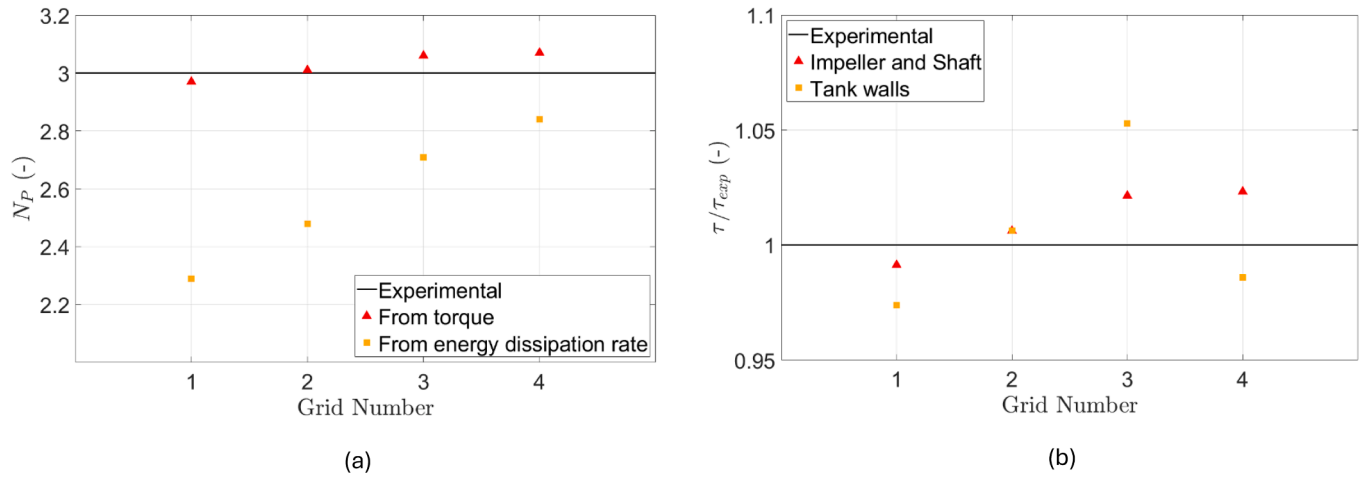

Fig. 3. Effect of increasing grid density on **(a)** the power number prediction from torque, $N_{P,t}$, and turbulent energy dissipation rate, $N_{P,\varepsilon}$; **(b)** the normalized torque on the rotating and stationary domains, obtained with the four grids mentioned in the text above – all for the ungassed condition.

equation (16) - is shown in Fig. 3-a. As expected, the difference between the $N_{P,t}$ and $N_{P,\varepsilon}$ decreases with an increase in the number of grid cells. Moreover, while the power based on the torque ($N_{P,t}$) is independent of the grid cells number after 3,889,328 cells, the power based on the energy dissipation rate, $N_{P,\varepsilon}$, is yet to achieve grid independence.

The torque on the rotating part and stationary parts of the tank has also been calculated separately and plotted in Fig. 3-b (the torque is normalized to the experimental torque calculated from $N_{P,u}$). Firstly, similar to what was reported in the literature [39,40] the power number on the moving wall achieved grid independence on a much coarser grid. Moreover, the plot shows that while the torque on the moving walls (impeller and shaft) increases with the number of cells, the power on the tank walls varies with no clear trend. Another important conclusion is that grid refinement did not help decrease the difference between the torque on the stationary and the torque on the rotating zone; on the contrary, the difference increased with grid refinement.

As mentioned earlier by Li et al. [78] and Maluta et al. [40], when modelling dispersion properties, correct prediction of the turbulent parameters may be of higher importance compared to the mean flow characteristics. In our case, however, although the energy dissipation rate improved with an increasing number of cells, the computational cost enforced by running the simulation on 17 million or 85 million grid cells was not feasible. Among the four grids studied here, the case with 3,889,328 cells, having an acceptable accuracy and reasonable computational cost (around 5–6 days of real-time simulation, using 128 cores in parallel), was chosen and used for the rest of the simulations (Fig. 2-b). However, it is important to keep in mind that using a medium number of grid cells may lead to an underprediction of the (overall) energy dissipation rate(s).

4.2.2. Two-Fluid simulation

For the MRF simulation, a pseudo-transient algorithm was used which is available when a coupled method is used for pressure–velocity coupling. While in the grid independence study, 2nd-order upwind was used for momentum and turbulent discretization (k and ε), when switching to a multiphase simulation, instabilities were observed especially in reaching air mass conservation. To avoid this, the 2nd-order discretization scheme was switched to the 1st-order for momentum, while the volume fraction was set to QUICK and k and ε were kept as 2nd-order [41]. As for the under-relaxation factors, the same authors recommended 0.3 for pressure, 0.4 for momentum, and 0.2 for the volume fraction.

Solving the equations for the two-fluid simulations of the stirred tank requires valid boundary conditions for both (quasi-)continuous phases. To avoid the high computational expenses that go with using a finer grid close to the sparger holes, the individual air inlet orifices of the sparger were replaced by a continuous surface set as the velocity inlet zone. The tank walls were no-slip, except for the impeller shaft revolving at the same absolute velocity as the impeller.

For the top surface (outlet), two boundary conditions have been widely used in the literature: pressure outlet and degassing. In our previous study on the small-scale 2 L bioreactor [9], the pressure outlet boundary condition was a better option due to the close distance of the impeller to the liquid surface and high impeller velocity. In this study, the bottom-mounted impeller has a lower speed and the distance between the impeller and the free surface is enough that no significant vortices are observed at the liquid surface. Therefore, a degassing boundary condition was used for the outlet. The impeller rotation was modelled using an MRF method that is suitable for large-scale bioreactors. The MRF simulations were run by using the pseudo-transient method with the constant default time-step.

4.3. M-Star simulation setup

The LB simulation uses a 2nd-order accurate explicit time-marching approach [79]. A lattice spacing (Δx) and a time step (Δt) should be defined to set up a simulation. The lattice spacing informs the smallest eddies and hydrodynamics length scales that will be captured explicitly by the simulation while the time step defines lattice velocity and compressibility of the liquid. Previous studies have suggested that a uniform lattice resolution of 100 points across the impeller diameter predicts converged and grid-independent power draw and blend time predictions [76]. A lattice study was also carried out starting from 100 lattice units and the power number results seem to be independent of lattice number after 200 lattice units, moreover, the available computational system failed to run the simulations when increasing lattices after 250. Regardless of the lattice numbers, the ungassed power draw and power dissipated were substantially larger than the values reported by the vendor. Furthermore, adding aeration to the vessel did not change the power draw significantly either. Based on these findings and given the size of the impeller being almost half the tank diameter, a lattice resolution of 200 points sufficed for the study of the tank.

Similar to the Fluent simulations, the time step was calculated based on the Courant-Friedrich-Lewy conditions that require the Co number to be smaller than 1.0. The time step in the current study was calculated based on $Co = 0.01$. This value proved to ensure that the lattice density fluctuations across the fluid remained below 2% [79,80]. The simulation took less than 1 h for 30 s of simulation time, on a single Tesla V100 GPU.

Being a Lagrangian-based code, the bubbles are modelled as discrete

Table 5
Summary of the cases used in the current paper (F denotes Fluent runs, and M refers to M−Star results).

Code	Case	$d_{B,i}$ (mm)	Remarks
Fluent	Case 1F*	3.54	Luo model for breakup and coalescence
	Case 2F*	3.54	Laakkonen for breakup, Prince & Blanch for coalescence
M−Star	Case 1M*	1.8	–
	Case 2M*	3.54	–
	Case 3M*	7.2	–

point objects that move obeying Newton's second law. The interphase forces comprise a gravity/buoyancy force as well as drag and added mass forces. The position and velocity of each bubble are solved by integrating the acceleration vector over time using a Verlet algorithm with the same time-step defined for the description of the fluid flow. Therefore, for coupling the two phases, a local body force is applied to each fluid voxel per the local gas volume fraction. This method which is referred to as the density method is chosen due to its lower computational costs and being less complicated.

In the M−Star solver, the mass and momentum conservation equations were solved using a single relaxation time Bhatnagar-Gross-Krook (BGK) operator on a D3Q19 lattice [79]. The top surface was modelled by the volume of fluid (VOF) approach [81]. The liquid phase interactions with the solid wall were described by a no-slip bounce-back algorithm. Bubbles entered the system through a continuous surface acting as the sparger with an initial size of 3.54 mm (as well as 1.8 mm and 7.2 mm). The displacement of the liquid surface after the start of the gas injection was modelled explicitly, meaning the level of the free surface rises with increasing the gas holdup.

The case studies in the current paper are summarized in Table 5 where names have been adopted to easily reference them across the paper (F denotes Fluent runs, and M refers to M−Star results).

5. Results and discussion

Given the considerations reported in Sections 1.2, 2.2, 4.2 (see *e.g.*, Fig. 3 on grid refinement) and 4.3, and given the more detailed assessments in our earlier paper on lab-scale bioreactors [9], we did not perform a new systematic and extensive sensitivity and validation study for the two-phase flow fields in the production vessel of current interest. Given our focus on mass transfer, we restrict ourselves to a detailed assessment of our simulation outcomes for gassed power draw (Section 5.1), air volume fraction (Section 5.2) and energy dissipation rate (Section 5.3) in this production vessel – as these make up the values of k_La (see Fig. 1) – before presenting and assessing the computational results on k_La in Section 5.4.

5.1. Power draw

Table 6 presents the CFD results obtained with Fluent and M−Star for the power draw P_t under gassed conditions alongside the ungassed power draw (P_u) reported by the vendor. Fluent predicts a gassed power draw slightly higher than the ungassed power draw reported by the vendor. As already mentioned in section 4.3, M−Star results for the aerated power draw were extremely larger than the vendor's ungassed value. A review of the available literature for elephant ear impellers [82,83] shows a decrease in the power draw is to be expected as a result of aeration, unlike what is obtained here from CFD. Note, however, that $P_t > P_u$was observed in the work of Bakker [84] for profiled A315 impellers and also reported by Devi and Kumar [23] for some of their dual impeller cases.

Since measured data for our elephant-ear impeller under gassed conditions is unavailable, a comparison was made with analytical correlations from the literature (although originally developed for Rushton turbines in smaller vessel sizes), as previously outlined in Table 3. Both the Hughmark [73] and the Michel and Miller [71] (with Abrardi et al. [72] constants) correlations predict an increase in the power number because of aeration, whereas the correlation of Michel and Miller [71] with constants obtained by Petříček et al. [31] predicted a 45% decrease in power draw as a result of aeration. Most of these correlations are closer to the P_t values found in M−Star simulations. One may expect that elephant-ear impellers have a lower Power number (see also Table 7) than the Rushton turbines (with typically Po ≈ 5) investigated by Hughmark [73] and Michel and Miller [71].

The general wisdom in the mixing community is that aeration results in a reduced power draw. Given the relatively low impeller speed (50 RPM) and very low gas flow rate (250 SLPM) in this study, an increase in power draw due to gassing as suggested by the Fluent simulations might be conceivable, at least has been reported earlier [84]. However, a 30–50 % increase as found in the M−Star simulations appears unusually high and might be attributable to numerical issues related to applying their Immersed Boundary Condition to the curved impeller blades mapped onto the orthogonal lattice.

Table 7
Comparison of the power number based on torque ($N_{P,t}$) and dissipated power number ($N_{P,\varepsilon}$) in CFD simulations.

	Case	$N_{P,t}$	$N_{P,\varepsilon}$
Fluent	Case 1F*	3.17	1.59
	Case 2F*	3.18	1.58
M−Star	Case 1M*	4.33	4.24
	Case 2M*	4.33	4.22
	Case 3M*	4.34	4. 17

Table 6
Comparison of the gassed power input in the tank calculated from torque (P_t) with analytical correlations ($P_{g,a}$) as suggested in Hughmark [73] and Michel and Miller [71] for Rushton turbines in smaller vessels.

Experimental		$P_u = 1100$ W				
	Cases	P_t(W)		Reference	$P_{g,a}$(W)	Remarks
Fluent	Case 1F*	1161		Hughmark [73]	1643	
M−Star	Case 2F*	1164	Analytical correlations	Michel and Miller [71]	1608	K_1, K_2, and K_3 from Abrardi et al.[72].
	Case 1M*	1585				
	Case 2M*	1573			601	K_1, K_2, and K_3 from Petříček et al.[31].
	Case 3M*	1582				

5.2. Energy dissipation rate

In general, it is expected that for a steady state condition, the input power to a system (P_t) is equal to the dissipated power calculated from the energy dissipation rate (P_ε) by use of equation (11). Here, the power number based on torque (input power number, $N_{P,t}$) is calculated and compared to the dissipated power for all the cases. The results are shown in Table 7. The Fluent results for $N_{P,\varepsilon}$ are underpredicted by some 45% compared to the input power number based on torque, $N_{P,t}$. This underprediction of the dissipated power in Fluent was expected due to the use of a RANS turbulence model (any $k-\varepsilon$), although the discrepancy is extremely large. Improvements may be achieved by employing a finer computational mesh and possibly by varying the discretization scheme, though this would increase computational expenses.

As for the dissipated power, $N_{P,\varepsilon}$, from M−Star, the time-averaged energy dissipation rate is not affected by bubble size and there is a good agreement between $N_{P,t}$ and $N_{P,\varepsilon}$. Better evaluation of the energy dissipation rate by M−Star was expected due to the use of the more

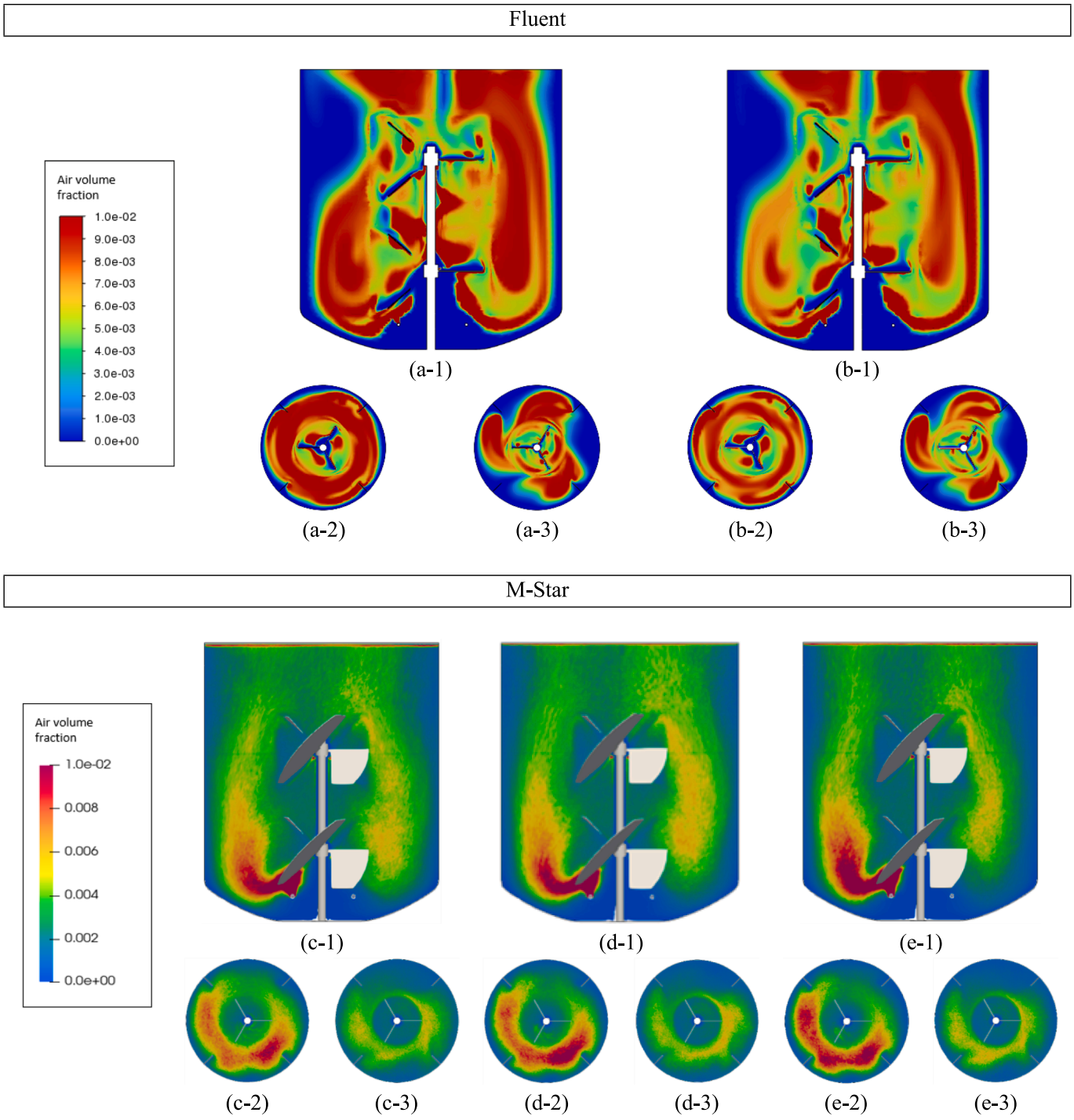

Fig. 4. The air volume fraction contour found in Fluent-PBM simulations with 14 bubble classes: **(a)** with the Luo breakup and coalescence model; **(b)** with the Laakkonen breakup and the Prince & Blanch coalescence model; and in M−Star simulations with breakup and coalescence: with **(c)** $d_{B,i} = 1.8$ mm, **(d)** $d_{B,i} = 3.54$ mm, and **(e)** $d_{B,i} = 7.2$ mm; all at **(1)** a vertical XY cross-section, **(2)** a horizontal cross-section at the level of the bottom impeller, and **(3)** a horizontal cross-section at the level of the top impeller.

accurate LES model for turbulence. Both the input power number and dissipated power number in the M−Star simulation, however, are much larger than the unaerated power number reported by the vendor and also from Fluent-PBM. This effect was also observed in single-phase simulations with M−Star, where the unaerated power was over-predicted compared to the value from the vendor.

The reason for this is not very well understood. Note that in itself LES does not require solving for the energy dissipation rate ε, differently from a RANS-based (two-fluid) simulation [85]. With the view of comparing P_ε with P_t, the (fluctuating and/or average) spatial ε − distribution needed for equation (11) has to be calculated in a post-processing routine. Whether or not equation (13) is a suitable way for calculating the unresolved dissipation rates, or even equation (14) is suitable to calculate the total ε, may require a more separate detailed assessment involving direct numerical simulations [75,85]. The apparent overestimation of power draw and dissipation rate may also be due to M−Star's IBM method for modelling the revolving elephant ear impeller in the regular Cartesian LB lattice. The combination of their IBM with the LES-SGS model and with equation (13), or equation (14), may also result in erroneous dissipation rates.

5.3. Air volume fraction

To take breakup and coalescence into account, different techniques are implemented in the two codes. In Fluent, the breakup and coalescence were included by using the PBM technique for 14 bubble classes with an initial bubble size of $d_{B,i} = 3.54$ mm, according to equation (6). To model breakup and coalescence, initially, Luo models were used, but due to a discussion with ANSYS, a Laakkonen model [42] was used for the breakup and a Prince and Blanch model [67] was used for coalescence. In M−Star, models for breakup and coalescence are added to the simulations while the initial bubble diameters are changed. Fig. 4 then shows the gas holdup contours for the Fluent-PBM cases as well as the M−Star cases with breakup and coalescence.

The difference between gas holdup as a result of changing the breakup/coalescence models is well distinguishable in our Fluent-PBM results, especially above the sparger on the left side of the tank, and in the bulk of the liquid. In M−Star, the overall effect of the breakup and coalescence is a rather more homogeneous distribution of air volume fraction throughout the tank for all three cases. Moreover, the time-averaged gas holdup changes only insignificantly because of changing initial bubble diameters, *i.e.* the gas holdup is independent of the initial bubble diameter.

Given the bubble number densities in the current reactor, one could wonder whether substantial agglomeration could take place anyhow. The kernel used in M−Star for bubble breakup centers on the so-called Hinze correlation which in each iteration step requires local ε − values to be calculated by means of the above commented equation (13). It looks as if the power draw and/or the (unresolved) ε- values are too high, leading to small(er) bubbles. On the one hand, it is just the strength of CFD that such detailed phenomena can be included, while on the other hand, no direct validation of these observations and trends is available.

In the Fluent-PBM simulations, the resulting bubble size distributions may be represented by the Sauter mean diameter, d_{32}. In Case 1F*, the Sauter mean diameter was reported to be 8.3 mm, which is in the same range previously reported by Haringa [86] and Günyol [74]. Changing the breakup and coalescence models in Case 2F* brings it to as low as 4.5 mm. In M−Star, regardless of the initial bubble size, the Sauter mean diameter predicted in all three cases is in the same range as reported by Scully et al. [1] in their Fluent-PBM simulation, around 1.8 times smaller than the values reported from our Fluent-PBM simulations in Case 2F*.

Smaller bubble sizes obtained in Case 2F* mean that higher gas holdup is to be expected since smaller bubbles have lower rise velocities and longer residence time. This, however, was not the case in the gas holdup contours from Fig. 4. One reason for this can be the local Sauter diameter range which is slightly increased from $0.2 < d_{32,local} < 13$ mm in Case 1F* to $0.2 < d_{32,local} < 15$ in Case 2F*.

The values of the Sauter mean diameters resulting from the simulations were compared to those calculated from correlations suggested by Calderbank [16] and Alves et al. [77]. Because the results from the Calderbank and Alves correlations are based on the gassed power input (P_g), substituting the different values for P_g obtained with the two codes results in different values for the bubble diameter: see Table 8. While the values of the Calderbank correlation are very close to that of M−Star, Fluent-PBM overpredicts the Sauter mean diameters because the energy dissipation rates are too low.

As for Alves et al. [77], also in Table 8, the correlations are divided into those in the impeller discharge region and those for the bulk of the tank. Understandably due to the high shear forces, bubbles are smaller in the impeller discharge region than in the bulk. The bubble sizes obtained for the discharge region, based on P_g from Fluent simulations, are close to the values obtained from Calderbank [16] and Miller [64]. However, for the M−Star data, considering larger values of the gassed power draw, smaller bubbles are obtained in the impeller discharge region of the tank compared to Fluent. These results are also closer to the Sauter mean diameters obtained from the simulations, especially for the impeller discharge region.

The extreme overprediction of the Sauter mean bubble diameter in Fluent-PBM simulations may be the consequence of using RANS turbulence models and too coarse a computational grid, both leading to an underprediction of energy dissipation rates and, therefore, breakup rates. It may also be due to a less suitable breakup/coalescence model. This uncertainty in bubble size and, therefore, gas volume fractions will translate to uncertainty in k_La values.

5.4. Volumetric mass transfer coefficient

The temporal development of volume-averaged k_La values during the Fluent-PBM and the M−Star simulations are shown in Fig. 5. The results from M−Star have been time-averaged over 60 s of simulation.

For the simulations carried out with breakup and coalescence in Fluent-PBM, the value of k_La is underpredicted by more than 70% when using the Luo model and by some 55 % when using the Laakkonen

Table 8
Comparison of the mean Sauter bubble size $d_{32,CFD}$ obtained from CFD simulations with breakup and coalescence with the analytically calculated values $d_{32,a}$ of the Sauter bubble diameter (surface-based bubble diameter ($\bar{d}_{32}$)) according to Calderbank [16] and the Sauter diameter in the impeller discharge region ($d_{32,ID}$) and in the bulk region ($d_{32,ID}$), respectively, according to Alves et al. [77]).

	Case	$d_{32,CFD}$ (mm)	$d_{32,a}$		
			Calderbank [16]	Alves et al. [77]	
			$\bar{d}_{32}$(mm)	$d_{32,ID}$(mm)	$d_{32,B}$(mm)
Fluent	Case 1F*	8.3	3.51	3.34	3.90
	Case 2F*	4.5	3.42	3.34	3.90
M−Star	Case 1M*	2.53	2.62	2.84	3.73
	Case 2M*	2.63	2.63	2.85	3.74
	Case 3M*	2.73	2.60	2.85	3.74

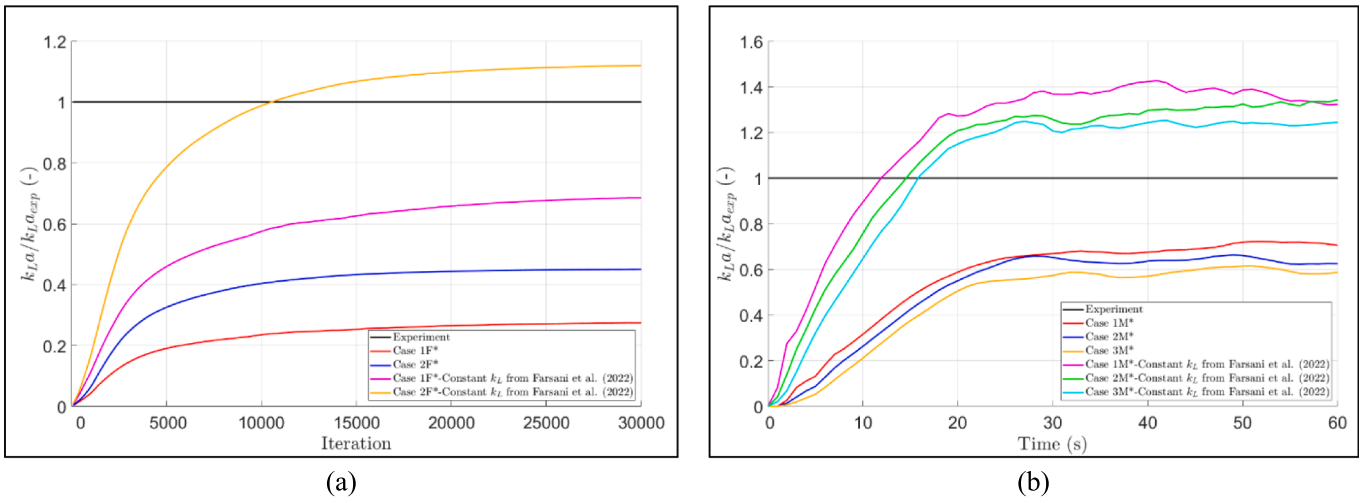

Fig. 5. Comparison of the k_La values for simulations with breakup and coalescence using Kawase-Moo-Young as well as constant k_L approach by Farsani et al. [37] ($k_L = 5 \cdot 10^{-4}$ m/s) in (a) Fluent and (b) M−Star.

Table 9
Comparison of the k_La obtained from CFD with the results obtained from analytical correlations by Calderbank (k_La_{Cal}) [35], Petříček et al. (k_La_{Pet}) [31], and from Calderbank and Moo-Young [25] and Farsani et al. [37] (k_La_{mod}).

Experiment		$k_La_{exp} = 11.5\ hr^{-1}$			
	Case	$k_La_{CFD}(hr^{-1})$	$k_La_{Cal}(hr^{-1})$	$k_La_{Pet}(hr^{-1})$	$k_La_{mod}(hr^{-1})$
Fluent	Case 1F*	3.1	20	20.4	7.8
	Case 2F*	5.2	20	20.4	12.8
M−Star	Case 1M*	8.1	22.6	25.5	15.5
	Case 2M*	7.2	22.6	25.4	14.7
	Case 3M*	6.7	22.6	25.5	14.0

breakup and the Prince and Blanch coalescence models. This is expected as the Sauter mean bubble size is smaller when using the Laakkonen breakup model compared to the Luo model. On the other hand, the energy dissipation rate did not change as a result of changing the breakup and coalescence models, meaning that the changes observed in k_La stem from changes in a rather than in k_L.

In M−Star, similar to the Sauter bubble diameter, changing the initial bubble size did not have a significant influence on the k_La. The k_La for the three bubble sizes was underestimated by around 40% when using breakup and coalescence. Considering that the turbulent energy dissipation rate remains unchanged as a result of changes in the initial bubble diameter (Table 7), the k_L value (calculated from the Kawase and Moo-Young correlation) should also remain unchanged. Therefore, the only reason for differences in k_La must again be in a. Increasing the initial bubble size did decrease the breakup/coalescence rates in the simulation, leading to a smaller a and, as yet, a lower k_La.

Results obtained for k_La based on the analytical correlations suggested by Calderbank [35] and by Petříček et al. [31] are also reported in Table 9. Both correlations substantially overpredict k_La compared to the experimentally measured value. While in the Fluent-PBM cases, the mean Sauter diameter in Case 2F* is smaller than in Case 1F* (*cf.* Table 8), k_La is the same according to just both correlations. Obviously, the influence of the Sauter mean bubble diameter on P_g is negligible, although the simulation predicts this effect to be rather significant.

Overall, k_La is affected by multiple factors, such as bubble dynamics, turbulence, and mixing efficiency, not just by power draw alone, and although empirical correlations such as those used here can provide a useful guideline, they only provide general trends based on specific reactor designs and operating conditions. Most of these correlations do not specifically relate to the elephant ear impeller and the operating conditions of the current bioreactor of interest. In addition, many of these empirical correlations have been derived for volume-averaged variables, while in CFD they are applied locally within the flow domain. Further, the two CFD codes used in this study exploit different turbulence models (two-fluid RANS *vs.* LES/Lagrangian), different approaches to gas volume fraction and bubble size distributions, different correlations for bubble coalescence and break-up, and different numerical methods including the type of grid and the treatment of the revolving impeller. No wonder that the two codes arrive at rather different values for k_La, based on conflicting values for power draw, energy dissipation rates, bubble size and gas volume fraction. In some cases, a deviation in a specific variable is compensated by an opposite deviation in another variable.

As previously mentioned, Calderbank and Moo-Young [25] and Farsani et al. [37] claimed k_L is independent of the energy dissipation rate and is just a function of physical properties. Farsani et al. [37] reported that this value is $5 \cdot 10^{-4}$ m/s and served as a lower limit for k_L in M−Star. Such a constant value implies that, at least at our very low aeration rates, the boundary layers about the bubbles may not so easily be affected by spatial and temporal variations in the energy dissipation rate outside this boundary layer. These variations may be too small and too fast given the response time of the boundary layers. In addition, the empirical nature of many engineering correlations restricts their general applicability (given the wide variation in impeller geometries and operating conditions). Rather than trusting that these empirical correlations allow for calculating local variables in CFD, we opted for just using a constant k_L, *viz.* $5 \cdot 10^{-4}$ m/s (according to [25,37]) and a volume-averaged interfacial area (from the simulations). We then found the moderated k_La (denoted as k_La_{mod}) values reported in Table 9, all being much closer to each other and to the experimentally measured k_La. In Fluent, we did have to use the recommended breakup and coalescence models in order to find this result.

Using a constant k_L and just the volume-averaged a from Fluent or M−Star improved the results significantly, which then are in good

agreement with the experimental k_La. This finding is remarkable given the different values for energy dissipation rates, power draw and bubble sizes as a result of differences in modelling. As long as the sole values of k_L or a are not measurable, one may not say for sure if the energy dissipation's role is significant or not. Questions about the relevance of the (spatially varying) energy dissipation rate and/or the suitability of all types of empirical correlations for use in CFD simulations remain unanswered, at least for the time being.

6. Conclusions

A set of CFD simulations was carried out by using a two-fluid version of a finite volume-based code, ANSYS-Fluent, as well as an LBM-based code with Lagrangian bubble tracking, M−Star. While the former is a RANS-based code exploiting a two-equation turbulence model, the latter uses the Large-Eddy Simulation (LES) technique. Because LESs produce inherently transient (dynamic) flow fields, they look therefore much more realistic. As M−Star exploits LB and runs on GPUs, it is substantially faster than the two-fluid Fluent code – another feature appealing to companies. In addition, M−Star tracks individual bubbles the number of which mainly depends on the aeration rate; bubbles are allowed to leave the liquid at the free surface. The two-fluid model of Fluent is in terms of the gas volume fraction which is one the variables to be resolved by the numerical method. Both codes require input on initial bubble size but optionally use quite different models to account for bubble breakup and coalescence.

As far as energy dissipation rate is concerned, Fluent produces too low values due to the use of a two-equation turbulence model, while M−Star arrives at values even higher than the power draw for unaerated conditions. In the perception of the authors, energy dissipation is a pending issue in CFD. This difference in energy dissipation rate results has a substantial impact on the values for the mass transfer parameters (see below).

Our main results on mass transfer which is the focus of this paper, are presented in four different sections, *viz.* on power draw, energy dissipation rate, gas volume fraction, and k_La, and then compared: mutually, with empirical correlations obtained from literature, and with an own experimental k_La value. We discuss in detail the practice of exploiting mass transfer correlations from the literature and their volume-averaged values for k_L and k_La in the spatially resolved flow fields calculed by CFD. The two codes arrive at rather different values for k_La, based on contradictory values for power draw, energy dissipation rates, bubble size and gas volume fraction. However, using a constant value for k_L and just the volume-averaged a from Fluent or M−Star improved the results significantly, which then are in better agreement with the experimental k_La.

In the meantime, CFD software can be used to assess trends, *e.g.* in learning about the effect of changing operating conditions. To guide future use of CFD with respect to aerated bioreactors for cell culture processes, our following more detailed findings may be helpful:

- The results obtained from simulations in Fluent predicted a slight increase in power draw (based on torque) as a result of aeration compared with the ungassed power draw specified by the impeller vendor. In M−Star, however, both power draws in unaerated and aerated cases are about the same, and extremely larger than the ungassed value reported by the vendor. These findings are opposite to the general consensus that aeration reduces power draw; only Bakker [84] reports a slight increase.
- The air volume fraction changed significantly in the bulk of the tank when in the Fluent/PBM simulations the breakup and coalescence models were changed from Luo models to the Laakkonen breakup model combined with the Prince and Blanch coalescence model. As a result, the Sauter mean diameter (d_{32}) was closer to those obtained from analytical correlations.
- In M−Star's bubble breakup/coalescence approach, the values for air volume fraction and d_{32} were independent of the initial bubble size. Overall, the Sauter mean diameter obtained from M−Star was the closest to the results obtained from analytical correlations.
- Based on the well-known fact that at a steady state, the power consumption based on the energy dissipation rates integrated across the liquid volume should be equal to the power draw based on the torque experienced by the impeller. Fluent underpredicted the integrated energy dissipation rate by some 45%, due to both using a RANS-based turbulence model and a rather coarse grid.
- M−Star predicted a close agreement between the power based on the torque and the dissipated power. These values, however, are 43% larger than the ungassed power number reported by the vendor. This huge overprediction may be due to the way M−Star calculates the unresolved (sub-grid scale) energy dissipation rates as well as to the immersed boundary condition used for simulating the revolving impeller in the regular lattice.
- The k_La values obtained with both codes were compared to our experimental value. All methods failed to predict the value of k_La accurately. In the Fluent-PBM simulation, using a Laakkonen breakup model with Prince and Blanch's coalescence model helped improve the results. In M−Star, the changes in the initial bubble diameter did not affect the value of k_La.
- Using a constant k_L value of $5 \cdot 10^{-4}$ m^{-1} and multiplying it by the volume-average interfacial area obtained from Fluent and M−Star helped improve the k_La results significantly. The k_La results from this method were in good agreement with the experimental k_La, while the Kawase-Moo Young correlation fails to predict the k_L accurately.

The above findings illustrate and imply that much more research is needed on both CFD specifics (such as a proper estimate of the energy dissipation rate) and on models for bubble coalescence and break-up and for mass transfer before reliable k_La values can be obtained from CFD simulations. In addition, the suitability of empirical correlations for volume-averaged quantities with the view of calculating local values in CFD needs further consideration.

CRediT authorship contribution statement

Roya Jamshidian: Writing – review & editing, Writing – original draft, Visualization, Validation, Software, Methodology, Investigation, Formal analysis. **James Scully:** Resources. **Harry E.A. Van den Akker:** Writing – review & editing, Supervision, Project administration, Conceptualization.

Declaration of competing interest

The authors declare that they have no known competing financial interests or personal relationships that could have appeared to influence the work reported in this paper.

Acknowledgements

The authors would like to acknowledge Regeneron Pharmaceuticals for funding this project and generously providing the experimental data essential to this study. Special thanks are also extended to Francisco Rodriguez of the Ireland ANSYS CADFEM support team as well as Johannes Wutz of M-Star support for their invaluable advice.

Data availability

Data will be made available on request.

References

[1] J. Scully, L.B. Considine, M.T. Smith, E. McAlea, N. Jones, E. O'Connell, E. Madsen, M. Power, P. Mellors, J. Crowley, Beyond heuristics: CFD–based novel multiparameter scale–up for geometrically disparate bioreactors demonstrated at industrial 2kL–10kL scales, Biotechnol. Bioeng. 117 (6) (2020) 1710–1723.

[2] F. Garcia-Ochoa, E. Gomez, Bioreactor scale-up and oxygen transfer rate in microbial processes: an overview, Biotechnol. Adv. 27 (2) (2009) 153–176.

[3] A. Bakker, H.E.A. Van den Akker, A computational model for the gas-liquid flow in stirred reactors, Trans IChemE, Part A, Chem Eng Res Des 72 (A5) (1994) 594–604.

[4] G. Lane, M. Schwarz, G. Evans, Modelling of the interaction between gas and liquid in stirred vessels, in: 10th European Conference on Mixing, Elsevier, 2000, pp. 197–204.

[5] A. Khopkar, A. Rammohan, V. Ranade, M. Dudukovic, Gas–liquid flow generated by a Rushton turbine in stirred vessel: CARPT/CT measurements and CFD simulations, Chem. Eng. Sci. 60 (8–9) (2005) 2215–2229.

[6] A.R. Khopkar, V.V. Ranade, CFD simulation of gas–liquid stirred vessel: VC, S33, and L33 flow regimes, AIChE J 52 (5) (2006) 1654–1672.

[7] J. Derksen, H.E.A. Van den Akker, Large eddy simulations on the flow driven by a Rushton turbine, AIChE J 45 (2) (1999) 209–221.

[8] H. Hartmann, J. Derksen, C. Montavon, J. Pearson, I. Hamill, H.E.A. Van den Akker, Assessment of large eddy and RANS stirred tank simulations by means of LDA, Chem. Eng. Sci. 59 (12) (2004) 2419–2432.

[9] R. Jamshidian, J. Scully, H.E.A. Van den Akker, Two–fluid simulations of an aerated lab–scale bioreactor, Chem. Eng. Res. Des. 196 (2023) 254–275.

[10] S. Mukherjee, A. Safdari, O. Shardt, S. Kenjereš, H.E. Van den Akker, Droplet–turbulence interactions and quasi-equilibrium dynamics in turbulent emulsions, J. Fluid Mech. 878 (2019) 221–276.

[11] R. Higbie, The rate of absorption of pure gas into a still liquid during short periods of exposure, Trans. Am. Inst. Chem. Engrs. 31 (1935) 365–389.

[12] R.B. Bird, E.N. Lightfoot, W.E. Steward, Transport phenomena, Wiley, 1960.

[13] E.L. Cussler, Diffusion: mass transfer in fluid systems, Cambridge University Press, 2009.

[14] J. Welty, G.L. Rorrer, D.G. Foster, Fundamentals of momentum, heat, and mass transfer, John Wiley & Sons, 2014.

[15] P. Danckwerts, Significance of liquid-film coefficients in gas absorption, Ind. Eng. Chem. 43 (6) (1951) 1460–1467.

[16] P. Calderbank, Physical rate processes in industrial fermentation. part 1: the interfacial area in gas-liquid contacting with mechanical agitation, Trans. Inst. Chem. Eng. 36 (1958) 443–463.

[17] S. Alves, C. Maia, J. Vasconcelos, Experimental and modelling study of gas dispersion in a double turbine stirred tank, Chem. Eng. Sci. 57 (3) (2002) 487–496.

[18] N. Frossling, Uber die verdunstung fallernder tropfen, Gerlands Beitr. Geophys. 52 (1938) 170–216.

[19] J.C. Lamont, D. Scott, An eddy cell model of mass transfer into the surface of a turbulent liquid, AIChE J 16 (4) (1970) 513–519.

[20] Y. Kawase, B. Halard, M. Moo-Young, Theoretical prediction of volumetric mass transfer coefficients in bubble columns for Newtonian and non-Newtonian fluids, Chem. Eng. Sci. 42 (7) (1987) 1609–1617.

[21] Y. Kawase, M. Moo-Young, Mathematical models for design of bioreactors: applications of: Kolmogoroff`s theory of isotropic turbulence, The Chemical Engineering Journal 43 (1) (1990) B19–B41.

[22] W. Pinczewski, S. Sideman, A model for mass (heat) transfer in turbulent tube flow. moderate and high Schmidt (Prandtl) numbers, Chem. Eng. Sci. 29 (9) (1974) 1969–1976.

[23] T.T. Devi, B. Kumar, Mass transfer and power characteristics of stirred tank with Rushton and curved blade impeller, Engineering Science and Technology, an International Journal 20 (2) (2017) 730–737.

[24] V. Santos-Moreau, J.C.B. Lopes, C.P. Fonte, Estimation of kLa values in bench–scale stirred tank reactors with self–inducing impeller by multiphase CFD simulations, Chem. Eng. Technol. 42 (8) (2019) 1545–1554.

[25] P. Calderbank, M.B. Moo-Young, The continuous phase heat and mass-transfer properties of dispersions, Chem. Eng. Sci. 16 (1–2) (1961) 39–54.

[26] S. Hänsch, D. Lucas, E. Krepper, T. Höhne, A multi-field two-fluid concept for transitions between different scales of interfacial structures, Int. J. Multiph. Flow 47 (2012) 171–182.

[27] F. Maluta, A. Paglianti, G. Montante, Two–fluids RANS predictions of gas cavities, power consumption, mixing time and oxygen transfer rate in an aerated fermenter scale–down stirred with multiple impellers, Biochem. Eng. J. 166 (2021) 107867.

[28] F. Maluta, A. Paglianti, G. Montante, Towards a robust CFD modelling approach for reliable hydrodynamics and mass transfer predictions in aerobic stirred fermenters, Biochem. Eng. J. 181 (2022) 108405.

[29] J. Smith, Scale-up of agitated gas-liquid reactors for mass transfer. Proc. of the 2nd European Conf. on Mixing, Cambridge, UK, 1977.

[30] K. Van't Riet, Review of measuring methods and results in nonviscous gas-liquid mass transfer in stirred vessels, Ind. Eng. Chem. Process Des. Dev. 18 (3) (1979) 357–364.

[31] R. Petříček, T. Moucha, F.J. Rejl, L. Valenz, J. Haidl, T. Čmelíková, Volumetric mass transfer coefficient, power input and gas hold-up in viscous liquid in mechanically agitated fermenters, Measurements and Scale-up, International Journal of Heat and Mass Transfer 124 (2018) 1117–1135.

[32] V. Linek, V. Vacek, P. Beneš, A critical review and experimental verification of the correct use of the dynamic method for the determination of oxygen transfer in aerated agitated vessels to water, electrolyte solutions and viscous liquids, The Chemical Engineering Journal 34 (1) (1987) 11–34.

[33] P. Havelka, T. Moucha, J. Sinkule, V. Linek, Chemical dynamic method for measuring kLa in gas-liquid dispersions, Chem. Eng. Commun. 168 (1) (1998) 97–110.

[34] L. Labík, T. Moucha, M. Kordač, F.J. Rejl, L. Valenz, Gas–liquid mass transfer rates and impeller power consumptions for industrial vessel design, Chem. Eng. Technol. 38 (9) (2015) 1646–1653.

[35] P. Calderbank, Physical rate processes in industrial fermentation. Part II—Mass transfer coefficients in gas–liquid contacting with and without mechanical agitation, Trans. Inst. Chem. Eng 37 (3) (1959) 173–185.

[36] A.A. Yawalkar, A.B. Heesink, G.F. Versteeg, V.G. Pangarkar, Gas—liquid mass transfer coefficient in stirred tank reactors, Can. J. Chem. Eng. 80 (5) (2002) 840–848.

[37] H.Y. Farsani, J. Wutz, B. DeVincentis, J.A. Thomas, S.P. Motevalian, Modeling mass transfer in stirred microbioreactors, Chem. Eng. Sci. 248 (2022) 117146.

[38] D.A. Deglon, C.J. Meyer, CFD modelling of stirred tanks: numerical considerations, Miner. Eng. 19 (10) (2006) 1059–1068.

[39] M. Coroneo, G. Montante, A. Paglianti, F. Magelli, CFD prediction of fluid flow and mixing in stirred tanks: numerical issues about the RANS simulations, Comput. Chem. Eng. 35 (10) (2011) 1959–1968.

[40] F. Maluta, A. Buffo, D. Marchisio, G. Montante, A. Paglianti, M. Vanni, Effect of turbulent kinetic energy dissipation rate on the prediction of droplet size distribution in stirred tanks, Int. J. Multiph. Flow 136 (2021) 103547.

[41] M. Elqotbi, S. Vlaev, L. Montastruc, I. Nikov, CFD modelling of two-phase stirred bioreaction systems by segregated solution of the Euler–Euler model, Comput. Chem. Eng. 48 (2013) 113–120.

[42] M. Laakkonen, P. Moilanen, V. Alopaeus, J. Aittamaa, Modelling local bubble size distributions in agitated vessels, Chem. Eng. Sci. 62 (3) (2007) 721–740.

[43] X. Li, K. Scott, W.J. Kelly, Z. Huang, Development of a computational fluid dynamics model for scaling-up Ambr bioreactors, Biotechnol. Bioprocess Eng. 23 (2018) 710–725.

[44] L. Niño, R. Gelves, H. Ali, J. Solsvik, H. Jakobsen, Applicability of a modified breakage and coalescence model based on the complete turbulence spectrum concept for CFD simulation of gas-liquid mass transfer in a stirred tank reactor, Chem. Eng. Sci. 211 (2020) 115272.

[45] T.K. Villiger, B. Neunstoecklin, D.J. Karst, E. Lucas, M. Stettler, H. Broly, M. Morbidelli, M. Soos, Experimental and CFD physical characterization of animal cell bioreactors: from micro-to production scale, Biochem. Eng. J. 131 (2018) 84–94.

[46] J. Sarkar, L.K. Shekhawat, V. Loomba, A.S. Rathore, CFD of mixing of multi–phase flow in a bioreactor using population balance model, Biotechnol. Prog. 32 (3) (2016) 613–628.

[47] R. Gelves, A. Dietrich, R. Takors, Modeling of gas–liquid mass transfer in a stirred tank bioreactor agitated by a Rushton turbine or a new pitched blade impeller, Bioprocess Biosyst. Eng. 37 (2014) 365–375.

[48] Y. Zhao, Lattice Boltzmann based PDE solver on the GPU, Vis. Comput. 24 (2008) 323–333.

[49] N. Hanspal, B. DeVincentis, J.A. Thomas, Modeling multiphase fluid flow, mass transfer, and chemical reactions in bioreactors using large–eddy simulation, Eng. Life Sci. 23 (2) (2023).

[50] J.A. Thomas, X. Liu, B. DeVincentis, H. Hua, G. Yao, M.C. Borys, K. Aron, G. Pendse, A mechanistic approach for predicting mass transfer in bioreactors, Chem. Eng. Sci. 237 (2021) 116538.

[51] J.A. Thomas, B. DeVincentis, N. Hanspal, R.O. Kehn, Predicting gas-liquid mass transfer rates in reactors using a bubble parcel model, Chem. Eng. Sci. 264 (2022) 118183.

[52] R. Clift, J.R. Grace, M.E. Weber, Bubbles, drops, and particles, Dover Publications, 2013.

[53] G. Montante, K. Lee, A. Brucato, M. Yianneskis, Numerical simulations of the dependency of flow pattern on impeller clearance in stirred vessels, Chem. Eng. Sci. 56 (12) (2001) 3751–3770.

[54] F. Maluta, A. Paglianti, G. Montante, Towards a CFD-PBE simulation of aerated stirred tanks at high gas hold ups and different flow regimes, Chem. Eng. Res. Des. 180 (2022) 425–436.

[55] F. Maluta, A. Paglianti, G. Montante, Prediction of gas cavities size and structure and their effect on the power consumption in a gas–liquid stirred tank by means of a two–fluid RANS model, Chem. Eng. Sci. 241 (2021) 116677.

[56] Z. Xing, G. Duane, J. O'Sullivan, C. Chelius, L. Smith, M.C. Borys, A. Khetan, Validation of a CFD model for cell culture bioreactors at large scale and its application in scale-up, J. Biotechnol. 387 (2024) 79–88.

[57] L. Shu, M. Yang, H. Zhao, T. Li, L. Yang, X. Zou, Y. Li, Process optimization in a stirred tank bioreactor based on CFD-Taguchi method: a case study, J. Clean. Prod. 230 (2019) 1074–1084.

[58] S. Mishra, V. Kumar, J. Sarkar, A.S. Rathore, CFD based mass transfer modeling of a single use bioreactor for production of monoclonal antibody biotherapeutics, Chem. Eng. J. 412 (2021) 128592.

[59] A. Wodołażski, Metaheurystic optimization of CFD–multiphase population balance and biokinetics aeration stirrer tank bioreactor of sludge flocs for scale-up study with bio (de/re) flocculation, Biochem. Eng. J. 184 (2022) 108477.

[60] C. Xu, X. Liu, C. Ding, X. Zhou, Y. Xu, X. Gu, Power consumption and oxygen transfer optimization for C5 sugar acid production in a gas-liquid stirred tank bioreactor using CFD-Taguchi method, Renew. Energy 212 (2023) 430–442.

[61] L. Niño, R. Gelves, J. Solsvik, Viscous effects on gas-liquid hydrodynamics for bubble size determinations in different Newtonian and non-Newtonian fluids using a CFD-PBM model, Chem. Eng. Sci. 282 (2023) 119324.

[62] S. Mishra, V. Kumar, J. Sarkar, A.S. Rathore, Mixing and mass transfer in production scale mammalian cell culture reactor using coupled CFD-species transport-PBM validation, Chem. Eng. Sci. 267 (2023) 118323.
[63] Ansys Fluent Theory Guide, 2022.
[64] D.N. Miller, Scale–up of agitated vessels gas–liquid mass transfer, AIChE J 20 (3) (1974) 445–453.
[65] H. Luo, Coalescence, breakup and liquid circulation in bubble column reactors, University of Trondheim, Norway, 1995. PhD Thesis.
[66] H. Luo, H.F. Svendsen, Theoretical model for drop and bubble breakup in turbulent dispersions, AIChE J 42 (5) (1996) 1225–1233.
[67] M.J. Prince, H.W. Blanch, Bubble coalescence and break–up in air–sparged bubble columns, AIChE J 36 (10) (1990) 1485–1499.
[68] C. Xing, T. Wang, K. Guo, J. Wang, A unified theoretical model for breakup of bubbles and droplets in turbulent flows, AIChE J 61 (4) (2015) 1391–1403.
[69] R. Andersson, B. Andersson, On the breakup of fluid particles in turbulent flows, AIChE J 52 (6) (2006) 2020–2030.
[70] R.P. Hesketh, A.W. Etchells, T.F. Russell, Experimental observations of bubble breakage in turbulent flow, Ind. Eng. Chem. Res. 30 (5) (1991) 835–841.
[71] B.J. Michel, S. Miller, Power requirements of gas–liquid agitated systems, AIChE J 8 (2) (1962) 262–266.
[72] V. Abrardi, G. Rovero, S. Sicardi, G. Baldi, R. Conti, Sparged vessels agitated by multiple impellers, Proc Eur Conf Mixing (1988) 329–336.
[73] G.A. Hughmark, Power requirements and interfacial area in gas-liquid turbine agitated systems, Ind. Eng. Chem. Process Des. Dev. 19 (4) (1980) 638–641.
[74] Ö. Günyol, Computational fluid dynamics of gassed-stirred fermenters, Delft University of Technology, 2017. PhD Thesis.
[75] J. Gillissen, H.E.A. Van den Akker, Direct numerical simulation of the turbulent flow in a baffled tank driven by a Rushton turbine, AIChE J 58 (12) (2012) 3878–3890.
[76] J.J. Giacomelli, H.E.A. Van den Akker, Time scales and turbulent spectra above the base of stirred vessels from large eddy simulations, Flow Turbul. Combust. 105 (1) (2020) 31–62.
[77] S. Alves, C. Maia, J. Vasconcelos, A. Serralheiro, Bubble size in aerated stirred tanks, Chem. Eng. J. 89 (1–3) (2002) 109–117.
[78] D. Li, Z. Gao, A. Buffo, W. Podgorska, D.L. Marchisio, Droplet breakage and coalescence in liquid–liquid dispersions: comparison of different kernels with EQMOM and QMOM, AIChE J 63 (6) (2017) 2293–2311.
[79] S. Succi, The lattice boltzmann equation: for fluid dynamics and beyond, Oxford University Press, 2001.
[80] J. Thomas, K. Sinha, G. Shivkumar, L. Cao, M. Funck, S. Shang, N.K. Nere, A CFD digital twin to understand miscible fluid blending, AAPS PharmSciTech 22 (2021) 1–14.
[81] P.-H. Chiu, Y.-T. Lin, A conservative phase field method for solving incompressible two-phase flows, J. Comput. Phys. 230 (1) (2011) 185–204.
[82] H. Zhu, A.W. Nienow, W. Bujalski, M.J. Simmons, Mixing studies in a model aerated bioreactor equipped with an up-or a down-pumping 'Elephant Ear' agitator: power, hold-up and aerated flow field measurements, Chem. Eng. Res. Des. 87 (3) (2009) 307–317.
[83] M. Botlagunta, V. Rewaria, P. Mathi, Oxygen mass transfer coefficient and power consumption in a conventional stirred-tank bioreactor using different impellers in a non-newtonian fluid: an experimental approach, Iran. J. Chem. Chem. Eng. 41 (2) (2022) 533–543.
[84] A. Bakker, Hydrodynamics of stirred gas-liquid dispersions, Delft University of Technology, 1992. PhD Thesis.
[85] H.E.A. Van den Akker, The Details of the Turbulent Flow Field in the Vicinity of a Rushton Turbine, 14th European Conference on Mixing, Warszawa EFCE event no. 711, Warsaw University of Technology, Faculty of Chemical and Process Engineering, 2012, pp. 485-496.
[86] C. Haringa, Through the Organism's eyes: the interaction between hydrodynamics and metabolic dynamics in industrial-scale fermentation processes, Delft University of Technology, 2017. PhD Thesis.